ELSEVIER

Contents lists available at ScienceDirect

Results in Physics

journal homepage: www.elsevier.com/locate/rinp





Passivation effect of NTCDA nanofilm on black phosphorus

Jia Liu^a, Shitan Wang^a, Baopeng Yang^a, Haipeng Xie^a, Han Huang^a, Dongmei Niu^{a,*}, Yongli Gao^b

- ^a Institute of Super-Microstructure and Ultrafast Process in Advance Materials, School of Physic and Electronics, Central South University, Changsha, Hunan 410012, China
- ^b Department of Physics and Astronomy, University of Rochester, Rochester, NY 14627, United States

ARTICLE INFO

Keywords:
Black phosphorus
Passivation
Photoelectron spectroscopy
Electronic structure

ABSTRACT

The environmental stability of black phosphorus (BP) is very important for its practical application. Here, we studied the protective effect of 1,4,5,8-naphthalenetetracarboxylic dianhydride (NTCDA) passivation layer on the BP against air exposure with photoemission spectroscopy (PES) and density functional theory (DFT) calculations. PES characterization manifests that NTCDA effectively extracts electrons in the BP valence band (VB) and increases the work function (WF) of BP. The PES results reveal a straddling gap (type-I) band alignment at the interface, accompanying with an interface dipole of 0.13 eV pointing from NTCDA to BP and band bending of 0.17 eV in BP. The charge transfer of 0.32 electron per molecule from BP to NTCDA is further confirmed by DFT calculations. Air exposure experimental results demonstrate that NTCDA can improve the environmental stability of BP and slow down the surface oxidation and degradation. Our work deepens the understanding of the passivation mechanism of BP and provides more experimental and theoretical insights for BP's surface modification and future applications in Two-dimensional (2D) devices.

Introduction

2D materials have received great attention owing to their extraordinary physical and chemical properties such as large specific surface area, high in-plane mechanical strength and excellent optoelectronic properties. 2D BP and its mono- and few-layer form are among the most addressed ones because of its unique properties. BP displays a layer tunable band gap that ranges between 0.3 eV and 2.0 eV [1] and carrier mobility of the order of $1000 \text{ cm}^2 \text{ V}^{-1} \text{ s}^{-1}$ [2]. The relatively weak van der Waal forces between interlayers and strong in-plane bonding forces enable BP to achieve seamless exfoliation similar to graphene and transition metal dichalcogenides (TMDs) [3,4]. BP has high anisotropy in electronic, optical [5,6] and thermal transport properties [7,8], which provide opportunities for conceptionally new devices [1,9,10]. The intrinsically direct band gap of electronic structures makes BP have broad application prospects in electronics, optical communication, and optoelectronic devices etc. [11-18]. However, the poor ambient stability due to reaction with oxygen and water in the environment results in rapid decomposition and property degradation [19-21]. It is therefore indispensable to develop protection methods for BP to overcome the bottleneck in its optoelectronic applications.

The passivation strategy can be divided into two categories, i.e. physical and chemical methods based on the interaction between BP and the protection layer. Despite the differences, achievements have been made in effective prevention of BP from swift oxidation in ambient with different materials. Functionalization with inorganic reagents in chemical methods is feasible. Caporali et al. reported a relevant enhancement of ambient stability in few-layer BP decorated with nickel nanoparticles as compared to pristine BP [22]. Additionally, the small n-type organic semiconductor molecules (OSCs) with conjugated structures are ideal for BP passivation layer because of, but not limited to the following advantages: 1) the electron deficient conjugate π skeleton can effectively withdraw the lone pair electrons of BP and decrease the reactivity of P atoms with oxygen; 2) the withdrawn electrons from BP are delocalized in the OSC conjugated π -skeleton and form a soft passivation; 3) the electronic structure of the molecules can be finely tuned by substituting the elements with other atoms or groups, i.e. fluoruration or chloruration, hence finely tune the interaction of the BP and molecular layer; and 4) the higher movability of the small organic molecules on BP makes self-assembling possible which is important for high quality mono-layer protection. Gusmão et al. reported that the noncovalent modification of BP with anthraquinone can effectively limit its degradation in

E-mail address: mayee@csu.edu.cn (D. Niu).

^{*} Corresponding author.

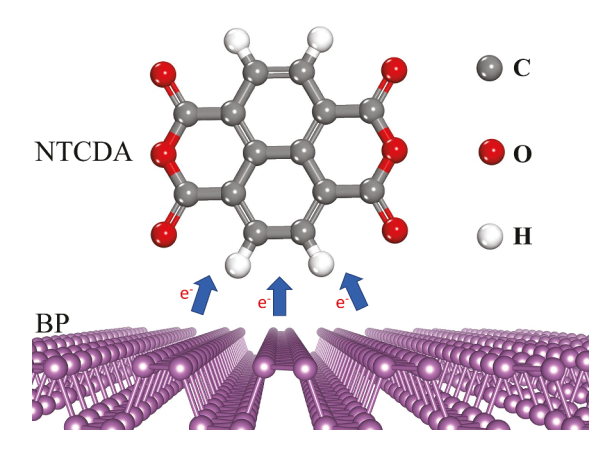


Fig. 1. NTCDA molecular structure and the scheme of the assembly reaction with BP.

atmospheric conditions [23]. Bolognesi et al. proposed that the BP-pyrene derivatives heterostructures can be stable in air for more than 6 months [24]. In theoretical calculations, the electrical, chemical and optical properties of BP were modified by introducing organic molecules such as PTCDA [25], TCNQ, tetrathiafulvalene (TTF) [26], tetracyanoethylene (TCNE) [27] and phenylenevinylene (PV) [28] onto BP surface. Zhao et al. proposed with DFT calculation that NTCDA could self-assemble into stable and close-packed networks to encapsulate BP [25]. NTCDA is a typical planar organic semiconductor material with 4 cyclic conjugated structures inside, and is often used as n-type material in semiconductor devices [29,30]. It is a strong electron acceptor which is expected to effectively withdraw the lone pair electrons of BP. However, there are few experiment studies on the electronic structure modification and film growth of NTCDA on BP, and most investigations are focus on the NTCDA-metal interface [31–36].

In this work, we prepared the NTCDA protection layer on BP (Fig. 1) and combined PES, atomic force microscopy (AFM), and DFT calculation to explore experimentally and theoretically how the NTCDA layer

modify the electronic structure of BP and its protection effect against oxygen. The results reveal a type-I band alignment at the NTCDA/BP interface and charge transfer from BP to NTCDA. The upward band bending in BP demonstrate that NTCDA p-dopped the BP and increase the WF of BP. DFT calculation shows that the VB and conduction band (CB) of the hetero junction maintains mainly the characteristics of BP and the interface state arise mainly from NTCDA. Air exposure experimental results show that NTCDA can improve the ambient stability of BP surface and slow down the surface oxidation and degradation, in excellent agreement with the DFT calculations that runs parallel with the experimental observation.

Experimental and theoretical details

Sample preparation and in-situ PES characterization were performed in a five-chamber ultrahigh vacuum system including an organic deposition chamber and an analysis chamber equipped with a hemispherical energy analyzer (SPECS PHOIBOS150), a microwave UV light source(He I=21.2 eV) and a monochromatic Microfocus X-ray Source (Al $K_{\alpha}=$ 1486.7 eV). More details of the system were given in our own previous publications [37-40]. The BP single crystal (HO Graphene) was mechanically cleaved in the load lock chamber with a scotch tape to ensure the cleaning of surface. Vacuum evaporation of NTCDA (Sigma-Aldrich) thin film was performed in organic molecular beam deposition chamber (base pressure: 1×10^{-8} mbar). The nominal thickness of deposited molecules was monitored by a quartz crystal microbalance in the OMBD chamber. The PES measurements were performed at room temperature with a hemispherical energy analyzer with the base pressure of batter than 2.0×10^{-10} mbar. Ultraviolet photoelectron spectroscopy (UPS) spectra were obtained with a bias of -5.0 V to enable the observation of the low-energy secondary cutoff edge. The core level spectra in X-ray photoelectron spectroscopy (XPS) were recorded with a pass energy of 40 eV. The AFM images of the samples were obtained in ambient using trapping mode of Agilent 5500AFM/SPM. The air exposure environment was in a dark environment with a relative humidity of 50%.

All DFT calculations were implemented in the Vienna ab initio

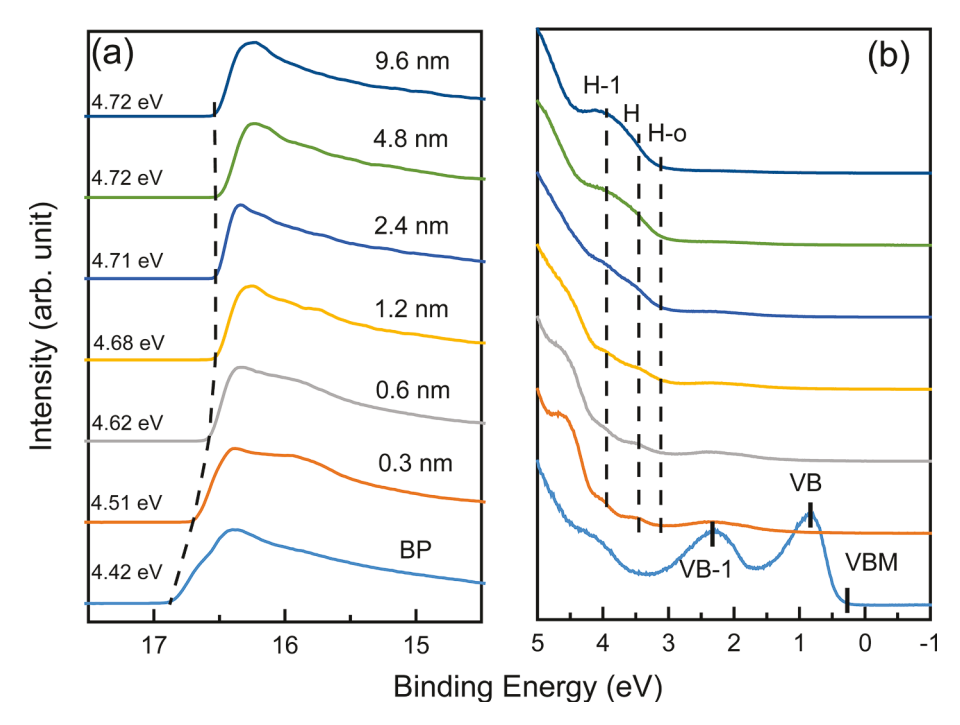


Fig. 2. Schematic Ultra-violet photoelectron spectra of NTCDA/BP heterostructures at increasing NTCDA coverage. (a) The secondary electron cutoff region reflects the work function change of the interface. (b) The VB region reflects the surface state of the interface. (For interpretation of the references to colour in this figure legend, the reader is referred to the web version of this article.)

J. Liu et al. Results in Physics 36 (2022) 105466

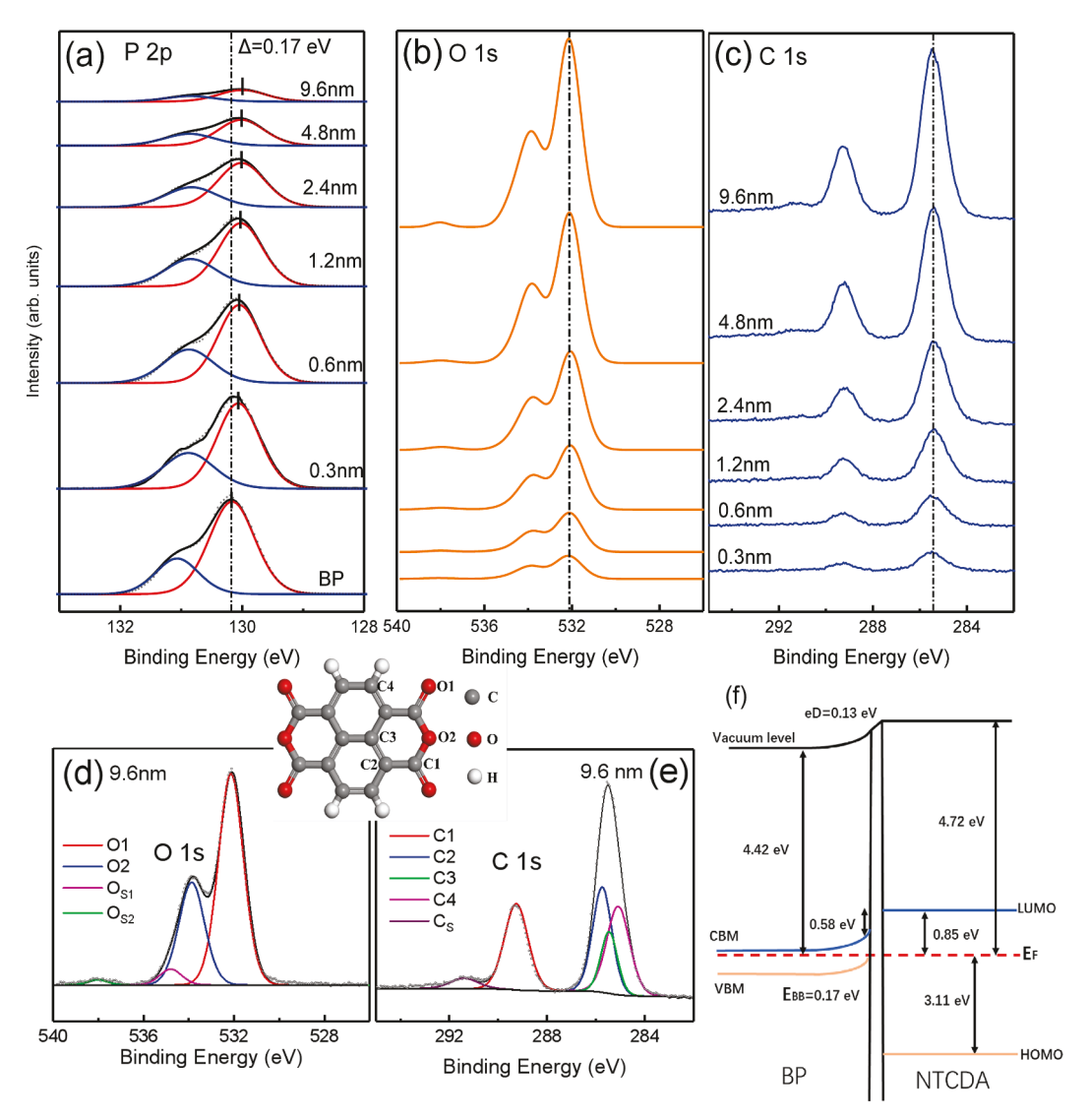


Fig. 3. XPS core level of (a) P 2p (b) O 1 s and (c) C 1 s for different coverage NTCDA on BP. The fitting curves of (d) O 1 s and (e) C 1 s core levels. The inset of (d-e) shows the molecular structure schematic of NTCDA molecule, the oxygen and carbon atoms in different chemical environments have been labeled. (f) The interface energy alignment of NTCDA/BP.

simulation (VASP) package [41] with the exchange-correlation functional [42] based on Perdew-Burke-Ernzerhof (PBE) generalized gradient approximation (GGA) [43]. The interaction between electron and ion was described by the projector augmented wave (PAW) potential [44]. The Monkhorst Pack scheme was used to sample the Brillouin zone [45]. Firstly, we optimized the structure of unit bulk BP. A mesh of $7\times2\times5$ k-point sampling was used for unit cell. The calculated lattice constants for bulk BP are a=3.30 Å, b=4.55 Å, and c=11.30 Å(Fig. S1a). The relaxed lattice constants for the single-layer BP are a =3.30 Å and b = 4.62 Å (Fig. S1b), in good agreement with previous studies [46]. To study the adsorption of NTCDA on the BP, a $4 \times 6 \times 1$ supercell containing 96P atoms was adopted, and a sizable vacuum layer of 20 Å isolated the neighboring periodic images of the BP slab (Fig. S1c). The six possible sites of adsorptions were considered (Fig. S2). A mesh of $7 \times 5 \times 2$ k-point sampling was used for bulk BP. To study the adsorption of NTCDA, a $4 \times 6 \times 1$ supercell containing 96P atoms was adopted, and a sizable vacuum layer of 20 Å isolated the neighboring periodic images of the BP slab. A mesh of $3 \times 3 \times 1$ k-point sampling was used for the BP slab and BP-NTCDA systems. The kinetic energy cutoff was set to be 500 eV for all the calculations. All structures were fully relaxed until the atomic forces on each atom were smaller than 0.02 eV $\rm \AA^{-1}$ and the total energy change was less than 1.0×10^{-5} eV. The effect

of van der Waals (vdW) interaction was accounted for by using empirical correction method proposed by Grimme (DFT-D2), which was a good description of long-range vdW interactions [47]. The adsorption energy was defined as: Ea = EBP-NTCDA – EBP – ENTCDA, where EBP-NTCDA, EBP, and ENTCDA represent the total energies of the NTCDA-adsorbed BP, the pristine BP, and the isolated NTCDA, respectively. The six optimized adsorption configurations of NTCDA molecule on BP are shown in Fig. S3. In order to estimate charge transfer between the NTCDA molecules and BP, we adopt Bader charge analysis method, using the Bader program of Henkelman's group [48].

Results and discussion

As the reactivity of the BP is determined by the frontier orbitals, we first examined the modification of the BP electronic structures by stepwise-deposited NTCDA cover layers with UPS measurements. As seen in Fig. 2, the secondary electron cutoff spectrum shows the sample WF value is 4.42 eV for pristine BP, which is consistent with previous report [49]. With NTCDA deposition, the WF increases by 0.3 eV and saturates at a nominal mass thickness of 12 Å. The change in the WF of the sample suggests that charge transfer and interface dipole occur at the interface. The VB, valence band maximum (VBM) and VB-1 of BP locate

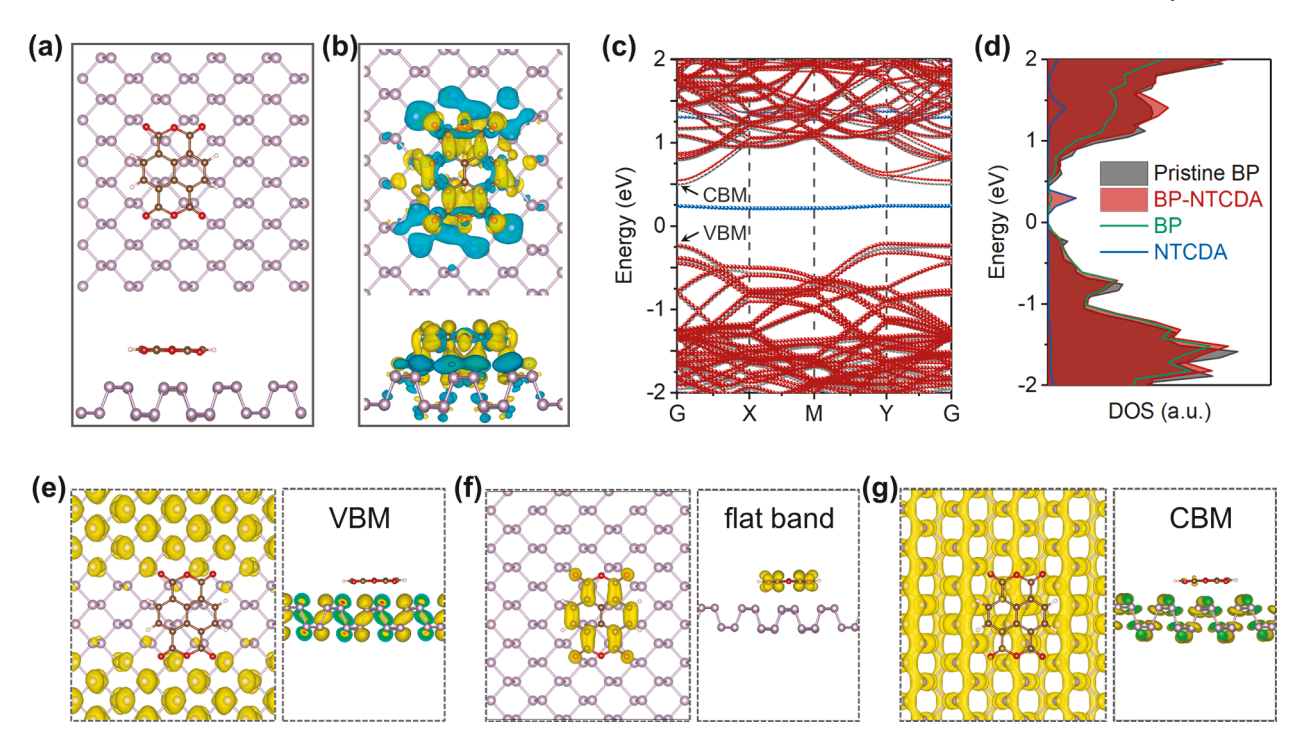


Fig. 4. (a) Top and side views of NTCDA adsorbed on BP. The P, C, H and O atoms of BP-NTCDA composite are represented by gray, brownness, white and red balls, respectively. (b) The charge density difference of NTCDA adsorbed on BP. The yellow and cyan volumes represent electron accumulation and depletion, respectively. (c) The calculated band structures of the pristine BP (gray dotted line) and the NTCDA-adsorbed BP (red and blue dotted lines) where red and blue lines record the contributions of BP and NTCDA, respectively. (d) The calculated DOS of the pristine BP (gray line) and BP-NTCDA composite (red line), and the PDOS of BP (green line) and NTCDA (blue line) for BP-NTCDA composite. The partial charge densities of (e) the VBM, (f) the flat band between VBM and CBM, and (g) the CBM for the BP-NTCDA composite. The isosurface corresponds to 0.0003 e Å⁻³. (For interpretation of the references to colour in this figure legend, the reader is referred to the web version of this article.)

at 0.83 eV, 0.25 eV and 2.32 eV, respectively. The intensity of the VB region is largely depressed after growing only 3 Å of NTCDA. The swift decrease of the signal from the VB area indicates adsorption of NTCDA molecules results in depletion of the electron in frontier occupied orbitals of BP. Meanwhile, the highest occupied molecular orbital (HOMO)-onset, HOMO and HOMO-1 of NTCDA appear and stay at 3.11 eV, 3.50 eV and 3.95 eV, respectively. The same HOMO region also appears on the thick layer [50] and on the weakly bound NTCDA monolayer on the GeS (001) substrate [51]. As the WF of NTCDA (4.72 eV) is greater than that of BP (4.42 eV) and the VBM of BP is close to the Fermi level of NTCDA, the electron transfer from VBM of BP to the NTCDA molecules is facilitated. This charge transfer causes the VB region to rapidly disappear at 3 Å of NTCDA deposition and electrons accumulate on the NTCDA side.

To analyze further the electron redistribution and the chemical environment changes across the interface, we perform the XPS measurement step by step. The full spectrum of different coverage of NTCDA on BP are presented in Fig. S4. The pristine P 2p core level can be separated into P 2p 1/2 (blue peak) at 131.05 eV and P 2p 3/2 (red peak) at 130.18 eV because of the spin orbit coupling as shown in Fig. 3(a). With increasing NTCDA coverage, the P 2p core level is gradually attenuated and shifted by 0.17 eV toward lower binding energy (BE), while the O 1 s and C 1 s peaks of NTCDA arise, as presented in Fig. 3(ac). The P 2p core level shift indicates that the adsorption of NTCDA induced band bending on the BP side because of the electrons transfer from BP to NTCDA. The O 1 s and C 1 s spectra are decomposed into several components with Lorentzian-Gaussion fitting [52]. The O 1 s core level includes two main components (O1 and O2) and two satellite peaks (O_{S1} and O_{S2}), as shown in Fig. 3(d). The O1 peak at 532.13 eV can be attributed to the oxygen atom of the carbonyl, O2 peak at 533.87 eV to the oxygen atom bridging the two carbonyl groups, and two satellites to the shakeup lines of O1 and O2 peaks. The ratio of O1:O2 is about 1.99:1, which agrees well with the oxygen atomic stoichiometric ratio of 2:1. Similarly, as shown in Fig. 3(e), there are four carbon components in the C 1 s core level, including C1 (289.26 eV, carbon atom in carbonyl), C2 (285.74 eV, carbon atom bonded with C1), C3 (285.46 eV, carbon atom in aromatic core), C4 (285.09 eV, carbon atom bonded with hydrogen atom) and satellite C_S [36]. The intensity ratio between four carbon components is also consistent with carbon atomic stoichiometric ratio ($I_{C1}:I_{C2}:I_{C3}:I_{C4}=2:2:1:2$). There are no additional components in the P 2p, O 1 s and C 1 s spectra, manifesting no new chemical bonds are formed between NTCDA molecule and BP. Those results are consistent with the UPS spectra and indicate the physisorption nature of NTCDA on RP.

To demonstrate clearly the energy level alignment of NTCDA/BP interface, we summarize the PES evolutions in Fig. 3(f). From the secondary electron cutoff area in UPS, the WF of BP and NTCDA on BP is found to be 4.42 eV and 4.72 eV. From the VB region in UPS, the position of the HOMO level of NTCDA is determined to be 3.11 eV below the Fermi level, and the VBM of BP locate at 0.25 eV. Taking the bandgap values of BP (0.35 eV) and NTCDA (3.96 eV) into consideration [50,53], the conduction band minimum (CBM) of BP and lowest unoccupied molecular orbital (LUMO) of NTCDA lies 0.1 eV and 0.85 eV above the Fermi level. The entire energy level of BP has an upward shift of 0.3 eV compared to the Fermi level. For the inorganic/organic interface, the shift of the vacuum level (Δ WF) is composed of two independent effects: band bending (E_{BB}) of the inorganic semiconductor surface and the interface dipole (eD) [54]. It can be confirmed from the P 2p core level shift that the E_{BB} on the BP side is 0.17 eV. The interfacial electron injection barrier from BP to NTCDA is reduced to 0.58 eV because of the upward band bending in BP side, and such a heterojunction interface can facilitate the interfacial electrons transport from BP to NTCDA. In addition, it is determined that there is an interface dipole of 0.13 eV pointing from NTCDA to BP side by calculating the remaining WF shift.

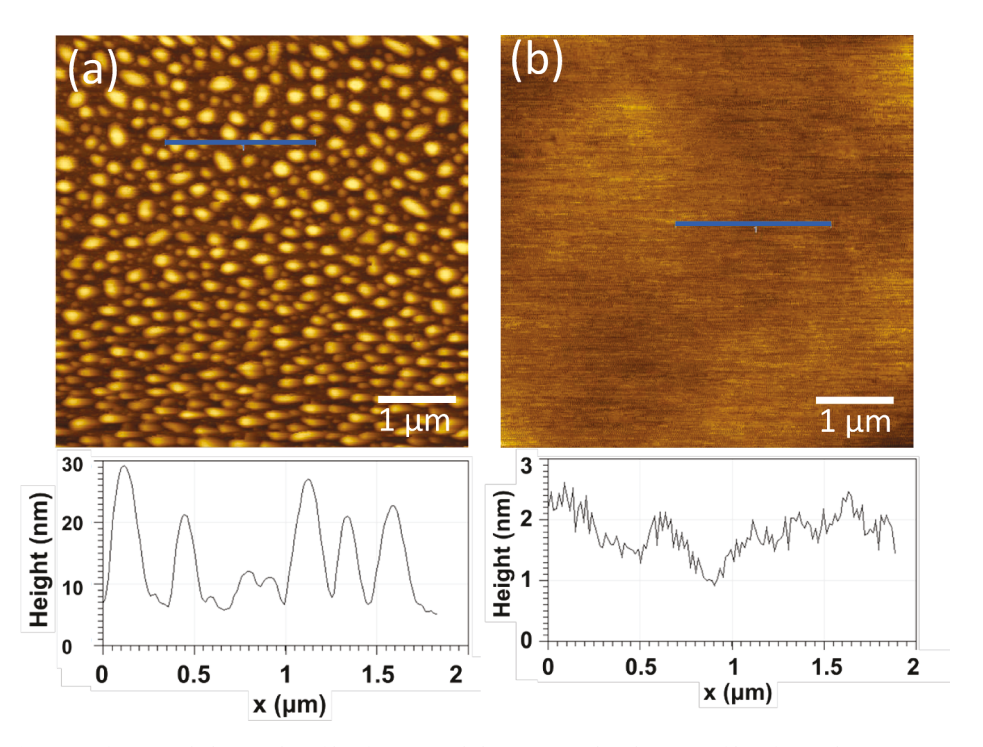


Fig. 5. Surface morphology and profile of (a) BP and (b) BP covered with NTCDA film after 24 h air exposure.

The interface dipole originates either from the assembly of polar molecules or the charge redistribution triggered by the deposition layer of electron affinity in large discrepancy with the substrate [55,56]. In this work, NTCDA is electron poor molecule with large electron affinity and can effectively cause electron transfer from BP forming an interface dipole pointing to BP.

To understand the redistribution of charge on the interface between NTCDA and BP, we carried out the DFT calculation. We considered six possible types of adsorptions (Fig. S2). The optimized adsorption configuration of NTCDA molecule on BP is shown in Fig. 4(a), which has higher adsorption energy than other adsorption configurations (Fig. S3). We investigated the charge transfer between NTCDA and BP through the charge density difference and Bader charge analysis. The charge density distribution of BP-NTCDA (Fig. 4b) shows that the charge mainly accumulated on NTCDA molecule and depleted on BP surface. The Bader charge analysis result shows that the charge transfer from BP to NTCDA molecule is 0.32 electron per molecule, indicating that the NTCDA molecule has strong electron withdrawing ability from the VBM of BP, which is consistent with the swift disappear of VB region in UPS spectra. In addition, we explored the effect of NTCDA on the electronic properties of BP. Fig. 4(c) shows the electronic band structures of BP with (red and blue) and without (gray) NTCDA adsorption. It is clearly portrayed in the figure that the red and gray dispersion curves of the CBM and VBM of BP is very similar before and after NTCDA adsorption. There is new flat blue band appears in the band gap around 0.25 eV, which arises from the lowest unoccupied state of NTCDA and attract the electron clouds at the interface from BP. We calculated the density of states (DOS) of the pristine BP and the projected density of states (PDOS) of the NTCDA adsorbed on BP to determine the origin of the flat band. As shown in Fig. 4(d), the DOS of the pristine BP (gray line) and BP-NTCDA composite (red line) almost completely overlap except for a peak at 0.25 eV, which correspond to the flat band in the band gap. Comparing the PDOS of pure BP (green line), pure NTCDA (blue line) and BP-NTCDA composite, we confirm that the flat band belongs to NTCDA and is almost independent of BP. This flat band act as a local scattering center which in general will reduce the mobility of carriers and enhance the recombination of light-excited electron-hole pairs [57]. We further analyzed the partial charge density of VBM, flat band and CBM, all illustrated Fig. 4(e-g) with yellow volumes representing electron accumulation. It shows that the charges of VBM and CBM nearly totally distributed on BP, while the flat band is mainly contributed by NTCDA. This means the NTCDA and BP are almost independent of each other. In other words, the adsorption of NTCDA basically will not break the electronic properties of the pristine BP. Meanwhile, we calculated the changes of BP work function (Fig. S5) and energy band (Fig. 4c) before and after the adsorption of NTCDA, and the results showed a trend consistent with the experiment (Table S1).

From the swift disappear of VB of BP at the deposition of 3 Å of NTCDA in UPS and calculated charge transfer of 0.32 electron per molecule to NTCDA in DFT, we can anticipate that by extracting valence electrons from the BP surface, NTCDA is possible to prevent BP from being oxidized by environment air. To preliminarily check the passivation effect of NTCDA molecule, surface morphology of bare BP and NTCDA-covered BP were characterized with AFM after 24 h air exposure. The surface morphology of BP after 24 h exposure is shown in Fig. 5(a). There are many bubbles with various sizes (0.05–0.5 μ m) and heights (2-22 nm) formed on the BP surface, indicating that severe degradation occurred on BP surface. The root-mean-square (RMS) roughness of bubbled BP surface is up to 8.36 nm, and the profile curve of blue line shows a maximum height of bubble is about 22 nm. The surface morphology changes of the BP are probably ascribed to the oxidation of BP. As the molar volume of phosphorus oxides is much larger than that of BP [58], oxidation may lead to volume increase and thus results in the expansion toward surface as bubbles. Kwak et al. explain that the exfoliated BP flake reacts with oxygen molecules once exposed to air, forming an inevitable thin phosphorus oxide (P₄ + 5O₂ \rightarrow P₄O₁₀) layers on the surface of the BP. The partially oxidized hydrophilic BP surfaces easily adsorb water molecules in the air and turn into phosphoric acid by the following reaction, $P_4O_{10} + 6H_2O \rightarrow$ 4H₃PO₄, which appears as topographic protrusions, or bubbles, on the BP surface [59]. It is hard to tune the component of the bubbles under certain atmosphere because of the inevitable chemical action, but one can prevent the degradation process by storing the BP in a nitrogen atmosphere to achieve surface protection by reducing contact with oxygen and water. On the contrary, the NTCDA-covered BP shows a much flatter surface morphology with a RMS roughness of 0.76 nm, as shown in

J. Liu et al. Results in Physics 36 (2022) 105466

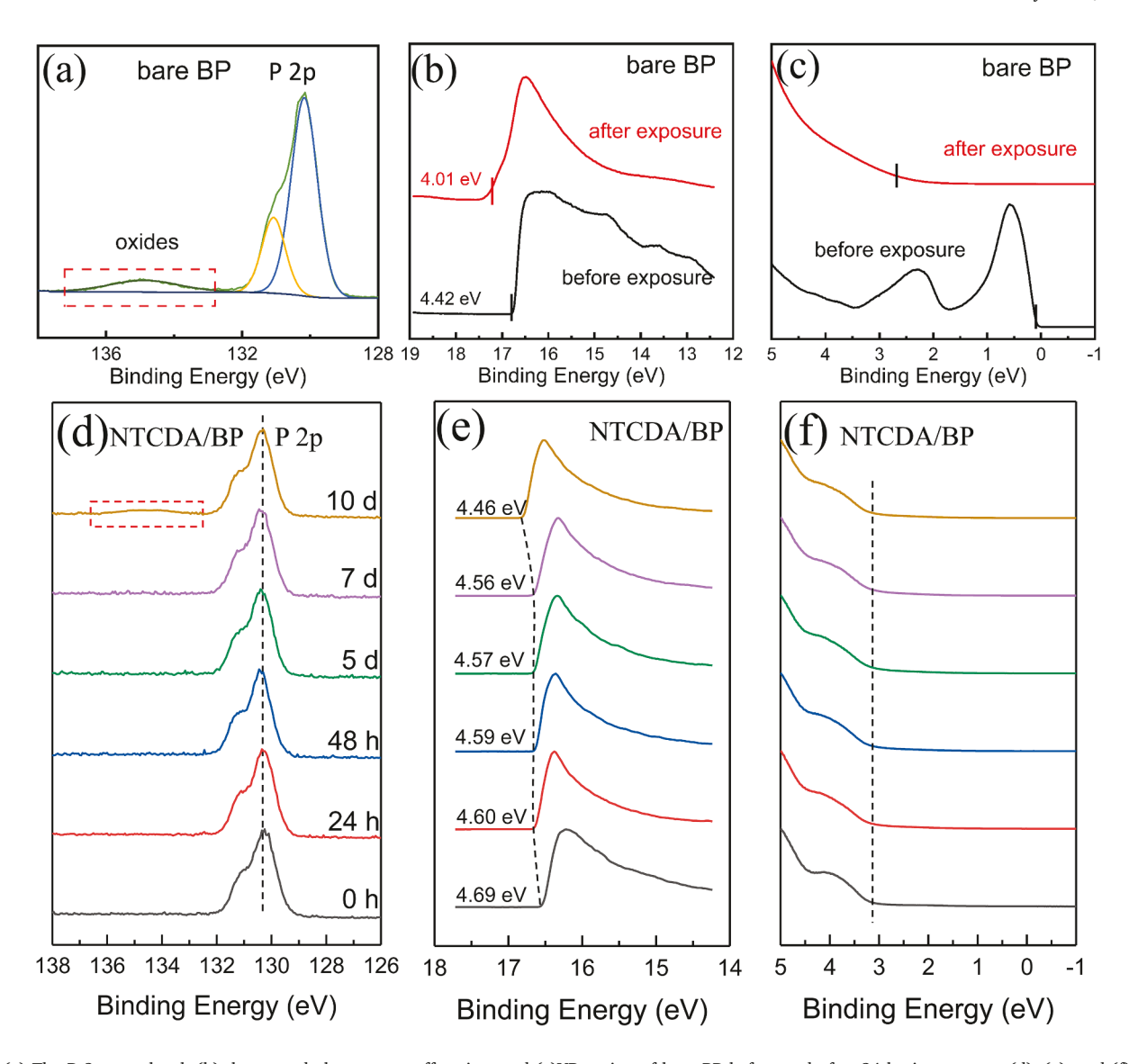


Fig. 6. (a) The P 2p core level, (b) the second electrons cutoff region, and (c)VB region of bare BP before and after 24 h air exposure. (d), (e), and (f) are the corresponding ones of NTCDA/BP at different air exposure levels.

Fig. 5(b). There are no bubble-like protrusions or other signs of degradation and the profile curve of 1 nm fluctuation indicates that the NTCDA film is compact and completely encapsulate the BP. Judging from the morphology of the NTCDA covered, the BP has no observable degradation on the morphology.

In order to analyze the component of the bubbles and examine the passivation effect of NTCDA molecules on BP, we performed PES characterization for the exposed bare BP and NTCDA-covered BP. The bubbled BP shows an extra component of P 2p emerged at 134.85 eV, 4.67 eV lower than pure P 2p, as shown in Fig. 6(a), which can be assigned to oxidation of BP. These results clearly proved that the phosphorus atoms on the surface have undergone significant oxidative degradation, consistent with the out-growing bubbles observed on AFM. In contrast, Fig. 6(d) shows that the NTCDA-covered BP contained a very pure P 2p peak at 130.18 eV without any additional components after 24 h, 48 h, 7 \times 24 h air exposure, implying that the underlying BP is pristine and is not corroded in the ambient. After 10 days of exposure, there is a weaker extra component of P 2p appeared, indicating the oxidative processes. As shown in Fig. 6(b-c), the cutoff edge of bare BP is broadened considerably and shifts by 0.41 eV towards the higher BE after 24 h exposure. Meanwhile, the electronic structure of the VB has changed significantly, with the original VB and VB-1 state completely

disappeared. The greatly changed cutoff region and VB region indicates that the BP surface has been severely oxidized [58] and destruction of the electronic structure occurred. However, UPS of NTCDA-covered BP after 24 h air exposure in Fig. 6(e-f) shows that the cutoff edge is still sharp with slight shift 0.09 eV, and HOMO structure of NTCDA is maintained at 3.09 eV, which confirms that exposure do not destroy the intrinsic electronic structure of NTCDA/BP. The results after air exposure for 7 days showed no significant shift in the cutoff edge and HOMO region of the interface, which indicated that the electronic structure of NTCDA/BP remained stable. In addition, we also investigated the effects of water and oxygen on the NTCDA/BP interface under illumination, and the results (Fig. S6) showed the same trend as NTCDA/BP in air exposure. Air exposure experiments manifested that NTCDA has improved the stability of BP in the ambient. One can anticipate that if the substrate temperature can be finely adjusted during the film growth [35,60] and the annealing [61] can be performed after the film is prepared, a much better NTCDA film quality may be achieved, and this may lead to a better passivation effect.

To understand the anti-oxidation mechanism of the NTCDA-covered BP surface, we calculated the physical and chemical properties of the $\rm H_2O+O_2/BP$ and $\rm H_2O+O_2/NTCDA/BP$ system by DFT calculation. Considering the computation time and coverage, we selected four $\rm H_2O$

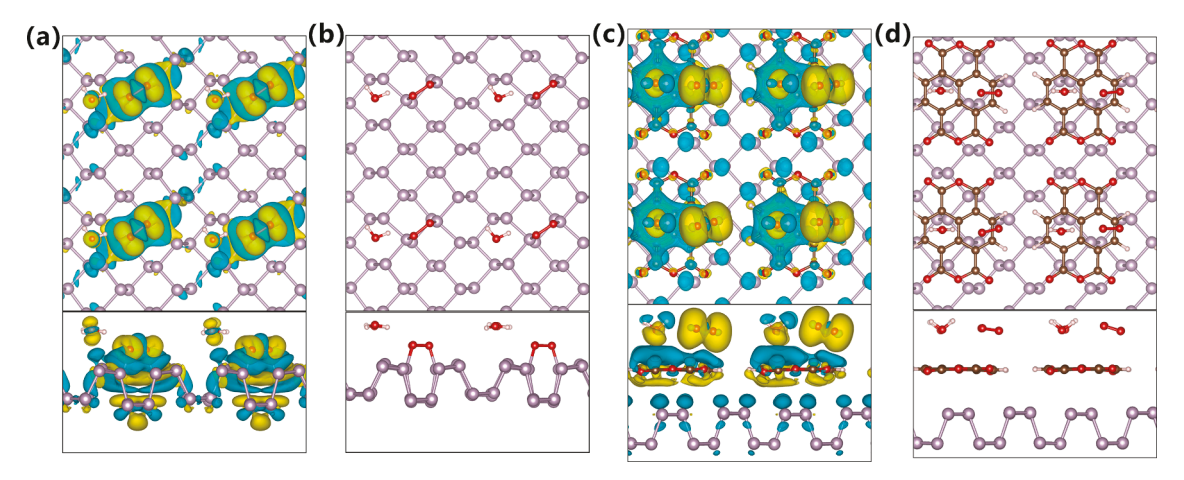


Fig. 7. (a) The charge density difference and (b) the optimized structures of $H_2O + O_2/BP$; (c) and (d) are the corresponding ones of $H_2O + O_2/NTCDA/BP$. The yellow and cyan volumes represent electron accumulation and depletion, respectively. The isosurface corresponds to 0.0003 e \mathring{A}^{-3} . The P, C, H and O atoms are represented by gray, brownness, white and red balls, respectively. (For interpretation of the references to colour in this figure legend, the reader is referred to the web version of this article.)

molecules, four O2 molecules and four NTCDA molecules. Shown in Fig. 7(a) are the charge density difference of $H_2O + O_2$ on BP. When H₂O + O₂ cluster are directly adsorbed on the surface of bare BP, the charge transfer from BP to H₂O + O₂ cluster is 0.25e. This charge redistribution may induce the formation of ${\rm O_2}^-$ anions and lower the reaction energy barrier of oxidation, to form phosphorous oxides. The formed P-O bonds at the optimized structure are indicated in red ball and sticks in Fig. 7(b). The formed phosphorous oxides will further degrade under the interaction of hydrogen bonds of water molecules and eventually destroy structure of BP [62]. However, it can be seen from Fig. 7(c) that the charge transfer from NTCDA to $H_2O + O_2$ cluster for $H_2O + O_2/NTCDA/BP$ system, which corresponds with the slight shift in the second electrons cutoff region of NTCDA/BP after 24 h air exposure as shown in Fig. 6(e). The P-O bonds is not observed in Fig. 7(d), indicating that the charge transfer from BP to $H_2O + O_2$ cluster is inhibited and the formation of phosphorous oxides is prevented, and it explains that NTCDA/BP has a very pure P 2p peak without any additional components after 24 h air exposure in Fig. 6(d). These results demonstrate that NTCDA monolayer can reduce the influence of H₂O + O₂ system on the electronic structure of BP, which are the crucial factors for effective passivation of the underneath BP.

Conclusion

In summary, we have prepared a passivation layer of NTCDA on BP surface with vacuum evaporation and have investigated the interfacial electronic structure and passivation effect by PES measurements, DFT calculations and AFM. The UPS and XPS confirmed the interfacial charge transfer from BP to NTCDA and band bending in BP side. A type-I band alignment is formed at NTCDA/BP interface. The electrons transport barrier from BP to NTCDA is 0.58 eV which can facilitate the interfacial electrical transport. In addition, a physisorption of NTCDA on BP can be recognized from the XPS examination as no new chemical bonds were observed. DFT calculations further demonstrated NTCDA molecules did not break the pristine electronic properties of BP and showed that NTCDA could effectively inhibit the charge transfer between BP and H₂O + O₂. PES measurements and AFM morphology studies demonstrate a stable and compact NTCDA thin film was at the surface of BP and the NTCDA-covered BP preserves its intrinsic chemical properties after 1 week of air exposure. Both PES characterization and DFT calculations showed that NTCDA can effectively extract lone pair electrons of BP to achieve chemical passivation, and denser covering of BP with NTCDA molecules by annealing or controlled film growth is expected to further suppress the formation of phosphorus oxides. In addition, we compared

the passivation effect of several organic passivation layers prepared by thermal evaporation, and the results show that the NTCDA passivation layer has the advantages of little influence on the intrinsic energy level of BP and better passivation effect (Table S2). Based on the protection effect of NTCDA on BP and its moderate influence on the electronic structure of BP, the application of NTCDA/BP is anticipated in high-performance organic-inorganic hybrid photovoltaic devices [63], field effect transistors [64,65], and possible heterojunction devices [66–68]. These results promise a simple method to passivate BP without affecting its electronic properties.

Author statement

In this paper, NDM and GYL provides main guidance and funding acquisition, LJ, WST and YBP work together to complete the specific investigation, experiments, analysis and communicates with WST, YBP, XHP, HH, NDM and GYL in the course of research. The data analysis and manuscript written carried out by both LJ and WST.

Declaration of Competing Interest

The authors declare that they have no known competing financial interests or personal relationships that could have appeared to influence the work reported in this paper.

Acknowledgements

This work was supported by the National Key Research and Development Program of China (Grant No. 2017YFA0206602) and the financial support from the National Natural Science Foundation of China (Grant Nos. 51173205 and 11334014). Y. Gao acknowledges the support of the National Science Foundation (Grant Nos. DMR-1903962). J. L. was supported by the Fundamental Research Funds for the Central Universities of Central South University (1053320211606).

Appendix A. Supplementary data

Supplementary data to this article can be found online at https://doi.org/10.1016/j.rinp.2022.105466.

References

 Cho K, Yang J, Lu Y. Phosphorene: An emerging 2D material. J Mater Res 2017;32 (15):2839–47.

- [2] Gusmão R, Sofer Z, Pumera M. Black Phosphorus Rediscovered: From Bulk Material to Monolayers. Angew Chem 2017;56(28):8052–72.
- [3] Mannix AJ, Kiraly B, Hersam MC, Guisinger NP. Synthesis and chemistry of elemental 2D materials. Nat Rev Chem 2017;1:0014.
- [4] Rezk AR, Walia S, Ramanathan R, Nili H, Ou JZ, Bansal V, et al. Acoustic-Excitonic Coupling for Dynamic Photoluminescence Manipulation of Quasi-2D MoS₂ Nanoflakes. Adv Opt Mater 2015;3(7):888–94.
- [5] Wu J, Mao N, Xie L, Xu H, Zhang J. Identifying the Crystalline Orientation of Black Phosphorus Using Angle-Resolved Polarized Raman Spectroscopy. Angew Chem 2015;127(8):2396–9.
- [6] Qiao J, Kong X, Hu Z-X, Yang F, Ji W. High-mobility transport anisotropy and linear dichroism in few-layer black phosphorus. Nat Commun 2014;5:4475.
- [7] Luo Z, Maassen J, Deng Y, Du Y, Garrelts RP, Lundstrom MS, et al. Anisotropic inplane thermal conductivity observed in few-layer black phosphorus. Nat Commun 2015;6(1). https://doi.org/10.1038/ncomms9572.
- [8] Łapińska A, Taube A, Judek J, Zdrojek M. Temperature Evolution of Phonon Properties in Few-Layer Black Phosphorus. J Phys Chem C 2016;120(9):5265–70.
- [9] Kim J-S, Liu Y, Zhu W, Kim S, Wu Di, Tao Li, et al. Toward air-stable multilayer phosphorene thin-films and transistors. Sci Rep 2015;5(1). https://doi.org/ 10.1038/srep.08989
- [10] Akhtar M, Anderson G, Zhao R, Alruqi A, Mroczkowska JE, Sumanasekera G, et al. Recent advances in synthesis, properties, and applications of phosphorene. npj 2D Mater Appl 2017;1(1). https://doi.org/10.1038/s41699-017-0007-5.
- [11] Luo S, Zhao J, Zou J, He Z, Xu C, Liu F, et al. Self-Standing Polypyrrole/Black Phosphorus Laminated Film: Promising Electrode for Flexible Supercapacitor with Enhanced Capacitance and Cycling Stability. ACS Appl Mater Interfaces 2018;10 (4):3538–48.
- [12] Wang Y, Zhang F, Tang X, Chen X, Chen Y, Huang W, et al. All-Optical Phosphorene Phase Modulator with Enhanced Stability Under Ambient Conditions. Laser Photonics Rev 2018;12(6):1800016. https://doi.org/10.1002/lpor. v12.610.1002/lpor.201800016.
- [13] Liu Y, Shivananju BN, Wang Y, Zhang Y, Yu W, Xiao Si, et al. Highly Efficient and Air-Stable Infrared Photodetector Based on 2D Layered Graphene-Black Phosphorus Heterostructure. ACS Appl Mater Interfaces 2017;9(41):36137–45.
- [14] Sun J, Lee H-W, Pasta M, Yuan H, Zheng G, Sun Y, et al. A phosphorene–graphene hybrid material as a high-capacity anode for sodium-ion batteries. Nat Nanotechnol 2015;10(11):980–5.
- [15] Wang M, Liang Y, Liu Y, Ren G, Zhang Z, Wu S, et al. Ultrasmall black phosphorus quantum dots: synthesis, characterization, and application in cancer treatment. Analyst 2018;143(23):5822–33.
- [16] Xu Y, Shi Z, Shi X, Zhang K, Zhang H. Recent progress in black phosphorus and black-phosphorus-analogue materials: properties, synthesis and applications. Nanoscale 2019;11(31):14491–527.
- [17] Avsar A, Vera-Marun IJ, Tan JY, Watanabe K, Taniguchi T, Castro Neto AH, et al. Air-Stable Transport in Graphene-Contacted, Fully Encapsulated Ultrathin Black Phosphorus-Based Field-Effect Transistors. ACS Nano 2015;9(4):4138–45.
- [18] Kamalakar MV, Madhushankar BN, Dankert A, Dash SP. Low Schottky Barrier Black Phosphorus Field-Effect Devices with Ferromagnetic Tunnel Contacts. Small 2015;11(18):2209–16.
- [19] Peng L, Abbasi N, Xiao Y, Xie Z. Black Phosphorus: Degradation Mechanism, Passivation Method, and Application for In Situ Tissue Regeneration. Adv Mater Interfaces 2020;7(23):2001538. https://doi.org/10.1002/admi.v7.2310.1002/ admi.202001538
- [20] Li Q, Zhou Q, Shi L, Chen Q, Wang J. Recent advances in oxidation and degradation mechanisms of ultrathin 2D materials in ambient conditions and passivation strategies. J Mater Chem A 2019;7:4291–312.
- [21] Zhao L, Chao X, Xu Na, Ling G, Zhang P. Strategies and Applications for Improving the Stability of Black Phosphorus in Physical Environment. Adv Eng Mater 2021;23 (10):2100450. https://doi.org/10.1002/adem.v23.1010.1002/adem.202100450.
- [22] Caporali M, Serrano-Ruiz M, Telesio F, Heun S, Verdini A, Cossaro A, et al. Enhanced ambient stability of exfoliated black phosphorus by passivation with nickel nanoparticles. Nanotechnology 2020;31(27):275708. https://doi.org/ 10.1088/1361-6528/ab851e.
- [23] Gusmão R, Sofer Z, Pumera M. Functional Protection of Exfoliated Black Phosphorus by Noncovalent Modification with Anthraquinone. ACS Nano 2018;12 (6):5666–73.
- [24] Bolognesi M, Moschetto S, Trapani M, Prescimone F, Ferroni C, Manca G, et al. Noncovalent Functionalization of 2D Black Phosphorus with Fluorescent Boronic Derivatives of Pyrene for Probing and Modulating the Interaction with Molecular Oxygen. ACS Appl Mater Interfaces 2019;11(25):22637–47.
- [25] Zhao Y, Zhou Q, Li Q, Yao X, Wang J. Passivation of Black Phosphorus via Self-Assembled Organic Monolayers by van der Waals Epitaxy. Adv Mater 2017;29(6): 1603990. https://doi.org/10.1002/adma.201603990.
- [26] Zhang R, Li B, Yang J. A First-Principles Study on Electron Donor and Acceptor Molecules Adsorbed on Phosphorene. J Phys Chem C 2015;119(5):2871–8.
- [27] Jing Yu, Tang Q, He P, Zhou Z, Shen P. Small molecules make big differences: molecular doping effects on electronic and optical properties of phosphorene. Nanotechnology 2015;26(9):095201. https://doi.org/10.1088/0957-4484/26/9/095201.
- [28] Li Q, Zhou Q, Niu X, Zhao Y, Chen Q, Wang J. Covalent Functionalization of Black Phosphorus from First-Principles. J Phys Chem Lett 2016;7(22):4540–6.
- [29] Zhu Mo, Liang G, Cui T, Varahramyan K. Depletion-mode n-channel organic fieldeffect transistors based on NTCDA. Solid State Electron 2003;47(10):1855–8.
- [30] Hammond WT, Xue J. Organic heterojunction photodiodes exhibiting low voltage, imaging-speed photocurrent gain. Appl Phys Lett 2010;97(7):073302. https://doi. org/10.1063/1.3481407.

- [31] Maruyama T, Hirasawa A, Shindow T, Akimoto K, Kato H, Kakizaki A. Energy-level alignment at NTCDA/metal and PTCDA/NTCDA interfaces studied by UPS. J Lumin 2000;87-89:782-4.
- [32] Tong Y, Fuhr JD, Martiarena ML, Oughaddou H, Enriquez H, Nicolas F, et al. Properties of NTCDA Thin Films on Ag(110): Scanning Tunneling Microscopy, Photoemission, Near-Edge X-ray Fine Structure, and Density Functional Theory Investigations. J Phys Chem C 2019;123(1):379–86.
- [33] Tonner R, Rosenow P, Jakob P. Molecular structure and vibrations of NTCDA monolayers on Ag(111) from density-functional theory and infrared absorption spectroscopy. PCCP 2016;18(8):6316–28.
- [34] Wießner M, Kübert J, Feyer V, Puschnig P, Schöll A, Reinert F. Lateral band formation and hybridization in molecular monolayers: NTCDA on Ag(110) and Cu (100). Phys Rev B 2013;88(7). https://doi.org/10.1103/PhysRevB.88.075437.
- [35] Schmidt T, Marchetto H, Groh U, Fink RH, Umbach E. Complex Monolayer Growth Dynamics of a Highly Symmetric Molecule: NTCDA on Ag(111). J Phys Chem C 2019;123(13):8244–55.
- [36] Tong Y, Nicolas F, Kubsky S, Oughaddou H, Sirotti F, Esaulov V, et al. Interplay between Structural and Electronic Properties in 1,4,5,8-Naphthalenetetracarboxylic Dianhydride Films on Cu(100). J Phys Chem C 2017;121(9):5050–7.
- [37] Liu Y, Zai H, Xie H, Liu B, Wang S, Zhao Y, et al. Effects of CsPbBr 3 nanocrystals concentration on electronic structure and surface composition of perovskite films. Org Electron 2019;73:327–31.
- [38] Yuan P, Liu Y, Xie H, Wei J, Zhao Y, Wang S, et al. Interfacial electronic structure at rubrene/NiFe heterostructure. Results Phys 2021;29:104692. https://doi.org/ 10.1016/j.rinp.2021.104692.
- [39] Zhao Y, Liu X, Li L, Wang S, Li Y, Xie H, et al. Modification of ultrathin C60 interlayer on electronic structure and molecular packing of C8-BTBT on HOPG. PCCP 2020;22:25264-71.
- [40] Xie H, Niu D, Zhao Y, Wang S, Liu B, Liu Y, et al. Photoemission studies of C8-BTBT/La_{0.67}Sr_{0.33}MnO₃ interface. Synth Met 2020;260:116261. https://doi.org/10.1016/j.synthmet.2019.116261.
- [41] Kresse G, Furthmüller J. Efficient iterative schemes for ab initio total-energy calculations using a plane-wave basis set. Phys Rev B 1996;54(16):11169–86.
- [42] Kohn W, Sham LJ. Self-Consistent Equations Including Exchange and Correlation Effects. Phys Rev 1965;140(4A):A1133–8.
- [43] Perdew JP, Burke K, Ernzerhof M. Generalized Gradient Approximation Made Simple. Phys Rev Lett 1996;77(18):3865–8.
- [44] Kresse G, Joubert D. From ultrasoft pseudopotentials to the projector augmentedwave method. Phys Rev B 1999;59(3):1758–75.
- [45] Monkhorst HJ, Pack JD. Special points for Brillouin-zone integrations. Phys Rev B 1976;13(12):5188–92.
- [46] Peng X, Wei Q, Copple A. Strain-engineered direct-indirect band gap transition and its mechanism in two-dimensional phosphorene. Phys Rev B 2014;90(8). https://doi.org/10.1103/PhysRevB.90.085402.
- [47] Klimeš J, Bowler DR, Michaelides A. Van der Waals density functionals applied to solids. Phys Rev B 2011;83(19). https://doi.org/10.1103/PhysRevB.83.195131.
- [48] Tang W, Sanville E, Henkelman G. A grid-based Bader analysis algorithm without lattice bias. J Phys: Condens Matter 2009;21(8):084204. https://doi.org/10.1088/ 0953-8984/21/8/084204.
- [49] Liu B, Xie H, Liu Y, Wang C, Wang S, Zhao Y, et al. Electronic structure and spin polarization of Co/black phosphorus interface. J Magn Magn Mater 2020;499: 166297. https://doi.org/10.1016/j.jmmm.2019.166297.
- [50] Chan CK, Kim E-G, Brédas J-L, Kahn A. Molecular n-Type Doping of 1,4,5,8-Naphthalene Tetracarboxylic Dianhydride by Pyronin B Studied Using Direct and Inverse Photoelectron Spectroscopies. Adv Funct Mater 2006;16:831–7.
- [51] Kera S, Tanaka S, Yamane H, Yoshimura D, Okudaira KK, Seki K, et al. Quantitative analysis of photoelectron angular distribution of single-domain organic monolayer film: NTCDA on GeS(001). Chem Phys 2006;325(1):113–20.
- [52] Bertóti I, Mohai M, László K. Surface modification of graphene and graphite by nitrogen plasma: Determination of chemical state alterations and assignments by quantitative X-ray photoelectron spectroscopy. Carbon 2015;84:185–96.
- [53] Asahina H, Shindo K, Morita A. Electronic Structure of Black Phosphorus in Self-Consistent Pseudopotential Approach. J Phys Soc Jpn 1982;51(4):1193–9.
- [54] Wang C, Niu D, Wang S, Zhao Y, Tan W, Li L, et al. Energy Level Evolution and Oxygen Exposure of Fullerene/Black Phosphorus Interface. J Phys Chem Lett 2018; 9(18):5254–61.
- [55] Gao Y. Surface analytical studies of interfaces in organic semiconductor devices. Mater Sci Eng R Rep 2010;68(3):39–87.
- [56] Ishii H, Sugiyama K, Ito E, Seki K. Energy Level Alignment and Interfacial Electronic Structures at Organic/Metal and Organic/Organic Interfaces. Adv Mater 1999;11(8):605–25.
- [57] Wang C, Niu D, Liu B, Wang S, Wei X, Liu Y, et al. Charge Transfer at the PTCDA/ Black Phosphorus Interface. J Phys Chem C 2017;121(33):18084–94.
- [58] Kim M, Kim H-G, Park S, Kim JS, Choi HJ, Im S, et al. Intrinsic Correlation between Electronic Structure and Degradation: From Few-Layer to Bulk Black Phosphorus. Angew Chem Int Ed 2019;58(12):3754–8.
- [59] Kwak D-H, Ra H-S, Yang J, Jeong M-H, Lee A-Y, Lee W, et al. Recovery Mechanism of Degraded Black Phosphorus Field-Effect Transistors by 1,2-Ethanedithiol Chemistry and Extended Device Stability. Small 2018;14(6):1703194. https://doi. org/10.1002/smll.v14.610.1002/smll.201703194.
- [60] Ng AMC, Djurišić AB, Chan WK. Organic luminescent nanowires: fabrication and characterization. In: Wang J, Lee C, Wang H, editors., Beijing, China: 2007, p. 682807.
- [61] Abdel-Khalek H, Shalaan E, El Salam M, El-Sagheer AM, El-Mahalawy AM. Effect of thermal annealing on structural, linear and nonlinear optical properties of 1, 4, 5,

- 8-naphthalene tetracarboxylic dianhydride thin films. J Mol Struct 2019;1178:
- [62] Zhou Q, Chen Q, Tong Y, Wang J. Light-Induced Ambient Degradation of Few-Layer Black Phosphorus: Mechanism and Protection. Angew Chem Int Ed 2016;55 (38):11437–41.
- [63] Wang Y, Zhang H, Zhang T, Shi W, Kan M, Chen J, et al. Photostability of MAPbI₃ Perovskite Solar Cells by Incorporating Black Phosphorus. Sol RRL 2019;3(9): 1900197. https://doi.org/10.1002/solr.v3.910.1002/solr.201900197.
- [64] Kim JS, Jeon PJ, Lee J, Choi K, Lee HS, Cho Y, et al. Dual Gate Black Phosphorus Field Effect Transistors on Glass for NOR Logic and Organic Light Emitting Diode Switching, Nano Lett 2015;15(9):5778–83.
- [65] He D, Qiao J, Zhang L, Wang J, Lan Tu, Qian J, et al. Ultrahigh mobility and efficient charge injection in monolayer organic thin-film transistors on boron nitride. Sci Adv 2017;3(9). https://doi.org/10.1126/sciadv.1701186.
- [66] Deng Y, Luo Z, Conrad NJ, Liu H, Gong Y, Najmaei S, et al. Black Phosphorus-Monolayer MoS₂ van der Waals Heterojunction p–n Diode. ACS Nano 2014;8(8): 8292–9.
- [67] Qin D, Chen L, Chen Y, Liu J, Li G, Quan W, et al. Enhanced performance in inverted organic light emitting diode assisted by an interlayer of crystalline and ndoped 1,4,5,8-naphthalene-tetracarboxylic-dianhydride: Enhanced performance in inverted organic light emitting diode. Phys Status Solidi A 2012;209(4):790–4.
- [68] He T, Li C, Zhang X, Ma Y, Cao Xu, Shi X, et al. Metalorganic Chemical Vapor Deposition Heteroepitaxial β-Ga₂O₃ and Black Phosphorus Pn Heterojunction for Solar-Blind Ultraviolet and Infrared Dual-Band Photodetector. Phys Status Solidi A 2020;217(2):1900861. https://doi.org/10.1002/pssa:v217.210.1002/pssa: 201900861